IEEE Access
Multidisciplinary ⋮ Rapid Review ⋮ Open Access Journal

Received 10 July 2024, accepted 30 July 2024, date of publication 5 August 2024, date of current version 13 August 2024.

Digital Object Identifier 10.1109/ACCESS.2024.3438464

RESEARCH ARTICLE

Development of an Automated Assistance System for Medication Compounding Work

JOANNE YOON[1], (Member, IEEE), YE-LIN KIM[2], AND YOUNG-BONG BANG[3,4], (Senior Member, IEEE)

[1]Biomedical Research Institute, Seoul National University Hospital, Seoul 03080, Republic of Korea
[2]Graduate School of Convergence Science and Technology, Seoul National University, Seoul 08826, Republic of Korea
[3]Department of Transdisciplinary Medicine, Seoul National University Hospital, Seoul 03122, Republic of Korea
[4]College of Medicine, Seoul National University, Seoul 03080, Republic of Korea

Corresponding author: Young-Bong Bang (ybbang@snu.ac.kr)

This work was supported by the National Research Foundation of Korea under Grant 2023R1A2C100660812.

ABSTRACT Antineoplastic medication compounding is conducted in most large hospitals and involves the repetitive task of extracting a specific quantity of medication from vials using syringes and transferring it into intravenous infusion bags. When a large syringe is used during medication compounding, manipulating the syringe plunger requires considerable force because of the negative pressure inside the vial as well as the viscosity of the drug solution. This repetitive and intense plunger manipulation can lead to musculoskeletal disorders of the arms, shoulders, and other areas. Implementing motorized syringe manipulation and automating the drug compounding process are beneficial approaches for enhancing pharmacist convenience and work efficiency. This study introduces the development of an automated assistance system for medication compounding designed to manipulate syringes and medication containers accurately and reliably. The developed equipment ensures compatibility with various syringes, vials, and intravenous (IV) infusion bags without the need for consumables. It is designed for the diversified, small-quantity production of personalized drugs, featuring a compact, affordable structure that can be easily accommodated within existing drug compounding facilities. The performance of the developed equipment is validated through simulations and experiments. The results prove the developed equipment has high dispensing accuracy (error range: $\pm 0.09\%$) and high repeatability (standard deviation: 21 mg).

INDEX TERMS Automated medical device, cavitation simulation, medication compounding, syringe gripping mechanism, syringe manipulation.

I. INTRODUCTION

Medication compounding refers to the process of blending two or more drugs according to a prescription or dispensing a single drug into specified quantities [1]. This process is aimed at preparing customized medication treatments for individual patients. The demand for personalized drug treatments, especially chemotherapy, is growing, emphasizing the critical need for precise and timely medication production [2].

Drug compounding typically involves several steps, beginning with the reconstitution of the drug solution by injecting a solvent into a vial containing the dried medicinal ingredient. Subsequently, a specific quantity of the prepared drug solution is extracted using a disposable syringe and injected into an intravenous (IV) infusion bag. In large hospitals, each pharmacist manually compounds medications for many patients, often having to repeat these tasks dozens of times or more per day.

Although extracting medication with a syringe may seem straightforward, considerable force is often required because of the negative pressure inside the vial, especially in the absence of proper air ventilation. Drug extraction becomes even more challenging when dealing with highly viscous medications, such as antineoplastic drugs, or when using a large syringe, resulting in high resistance while pushing or pulling the plunger [3]. Repetitive syringe manipulation

The associate editor coordinating the review of this manuscript and approving it for publication was Hassen Ouakad.

(a) (b) (c)

FIGURE 1. Commercial products to assist syringe manipulation for medication compounding. (a) Syringe drive/pump [5]. (b) Automated dispensing machine [6]. (c) Robotic compounding system [7].

leads pharmacists to experience strain on their wrists, which can result in musculoskeletal disorders of the arms and shoulders [4].

The posture of handling a syringe is also a factor that strains the user's wrist. Pharmacists adopt a specific posture to prevent air from entering the syringe: they hold the syringe vertically upward, ensuring that the needle tip remains fully immersed in the drug solution, and then slowly pull the plunger to draw the medication from a vial. This procedure requires them to hold the vial and syringe barrel with one hand while controlling the syringe plunger with the other. Maneuvering a syringe with only one hand is highly inconvenient, especially when using a large syringe, as it can apply pressure to the user's wrist.

Automating syringe manipulation, the most critical and demanding task in the compounding process, can improve the convenience of pharmacists and relieve their heavy workload and physical fatigue. Employing properly automated equipment can not only increase work efficiency but also ensure consistent medication compounding quality (including dosage accuracy and precision), regardless of the pharmacists' skill level. Additionally, it can decrease the exposure to hazardous drugs, such as anticancer medications, and lower the risk of accidents, such as needle sticks.

Commercial equipment for syringe manipulation and medication compounding are classified into three types, as shown in Fig. 1. The first type is the syringe drive/pump (Fig. 1(a)), a straightforward device equipped with a linear actuator designed only to push and pull a syringe plunger [5], [8], [9], [10], [11], [12]. This device is commonly used for infusing drugs at a constant flow rate over a user-set period using a prefilled syringe and is not suitable for drug compounding purposes.

An automated dispensing machine (ADM, Fig. 1(b)) is more appropriate for compounding than a syringe drive/pump [6], [13]. This medium-sized benchtop machine is designed for use within a biological safety cabinet (BSC) for sterile drug preparation. To use the ADM, a vial and an IV bag must first be connected to a syringe with consumables such as tubes and check valves. Once all parts are connected, the ADM transfers the medication in the user-set quantity from the vial to the IV bag using the syringe. A typical ADM is equipped with one or more drug-delivery channels, each designated for a specific syringe size. If a syringe that is not matched for the channel is used, it cannot be installed, or the channel actuator will need to be recalibrated for the syringe.

ADM may be useful for repetitive tasks involving dispensing a single drug into many IV bags; however, it is not suitable for mixing multiple drugs for personalized medication preparation, which is a near-universal constant in healthcare facilities. This is because of the frequent need for consumable changes, which not only decreases the efficiency of compounding work but also leads to significant wastage owing to residual medicine in consumables, such as tubes and connectors.

The last type is a robotic compounding system (RCS, Fig. 1(c)), in which the robot automatically conducts the entire process of conventional manual drug compounding [7], [14], [15], [16], [17], [18]. The RCS comprises one or two robotic arms and several auxiliary devices, integrated into a large cabinet, thus requiring a large installation space. Owing to its advanced automation, RCS offers accuracy and convenience; however, it also has complexities and substantial costs. Furthermore, its operational speed is comparatively slower than that of manual compounding methods. Large hospitals that handle a high volume of medication compounding often find it challenging to depend solely on RCS, mostly requiring parallel use of manual methods.

To overcome the limitations of both commercial ADM and RCS, this study introduces novel equipment for medication compounding, incorporating the following features:

- Syringe manipulation and dispensing of the drug solution from the vial to the IV bag are automatically performed.
- It is equipped with a suitable gripping and driving mechanism to enhance the accuracy and stability of the syringe manipulation.
- Various syringes, vials, and IV bags are compatible, allowing flexible application in different medication-compounding cases.
- Operating costs are reduced by eliminating the need for consumables to connect the syringe and drug containers, and no drugs remain in the connecting parts. This feature is crucial for the diversified, small-quantity production of personalized drugs.
- It includes a function to reduce the occurrence of cavitation when extracting the drug solution using a syringe.
- With its compact size and affordability, it can be easily accommodated within existing drug compounding facilities and a typical BSC workbench. Thus, each pharmacist can conveniently access it whenever required.

The remainder of this paper is organized as follows. In Section II-A, the detailed design requirements are reviewed, and in Section II-B, notable features of the mechanical system of the proposed equipment are introduced. In Section II-C, the performance of the designed mechanical

system is examined using kinematic and static analyses. In Section II-D, the structure and function of the control system are outlined. Section II-E focuses on the syringe plunger control method to prevent cavitation within a syringe. Finally, the performance of the developed prototype is verified through experiments, as described in detail in Section III.

II. MATERIALS AND METHODS

A. REQUIREMENTS FOR DESIGN

We visited the medication compounding facility at the Seoul National University Hospital to investigate the compounding work process and environment. Furthermore, through several meetings with pharmacists responsible for preparing anticancer injections, we identified detailed design requirements as follows:

- *Size of equipment:* For sterile preparations of hazardous drugs, such as anticancer drugs, a BSC is used to prevent drug contamination and spread. The BSC workbench is equipped with various auxiliary devices for drug preparation (e.g., multiple syringes, vials, IV bags, and a repeater pump for solvent injection for drug dissolution); therefore, there is not much available space. For this reason, the overall size of the equipment must be sufficiently small to be placed on a typical BSC workbench: the more compact it is, the more useful it is. Fig. 2 shows an example of the BSC: Esco Lifesciences group's Class 2 Type A2, with a workbench width ranging from 970 to 2440 mm, a depth of 623 mm, and a height of 690 mm [19].
- *Size of disposable syringes:* Multiple syringe sizes, typically up to 50 mL, are used for drug compounding. Syringes under 20 mL have a small plunger driving force, making them easy to manipulate, whereas those over 20 mL have tough plunger driving resistance, making them difficult to manipulate. Therefore, developing a syringe manipulation device capable of handling 20–50 mL syringes could greatly enhance the convenience of pharmacists.
- *Type and geometry of vials:* Vial openings have various shapes, but the most commonly used type is the standard form capped with a rubber stopper and an aluminum cap. The volume of vials used for drug compounding is generally within the range of 5–50 mL. The dimensions of the vial vary depending on its capacity, but the dimensions of the opening and bottleneck are standardized (ISO 8362-1:2018). Therefore, when developing a vial gripper, it is necessary to consider the geometric features of standard vials of various capacities.
- *Type and geometry of intravenous infusion bags:* Intravenous infusion bags (IV bags) typically have two ports: one is a patient access spike port, and the other is an injection port for adding medication. The injection ports are generally shaped like cylinders, whereas some ports have a polyhedral shape (Fig. 3). Therefore, it is necessary to develop a compatible gripper for IV bags of various port shapes.
- *Syringe gripping mechanism:* In the case of the syringe drive/pump or ADM mentioned in the introduction, their syringe holders (or fixtures) typically feature slots for inserting the syringe barrel flange or plunger flange. Although installing the syringe into the slot is simple and easy, some syringes may fit tightly, whereas others may fit loosely, depending on their flange thickness deviation. The dimensional gap between the syringe flange thickness and slot width is highly related to plunger control accuracy and drug dose errors during extraction and injection. Thus, there is a need to develop an advanced syringe gripping mechanism.

FIGURE 2. Example of a biological safety cabinet (BSC) [19].

FIGURE 3. Various port shapes of intravenous (IV) bags.

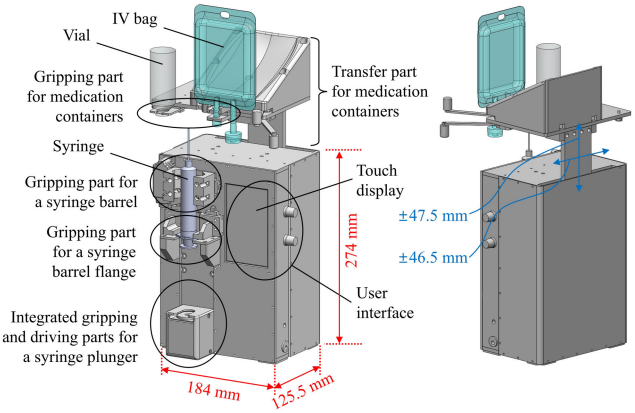

FIGURE 4. Structure of the designed equipment.

B. MECHANICAL SYSTEM DESIGN

Fig. 4 shows the machine structure [20]. The equipment has a syringe gripping mechanism that can stably and

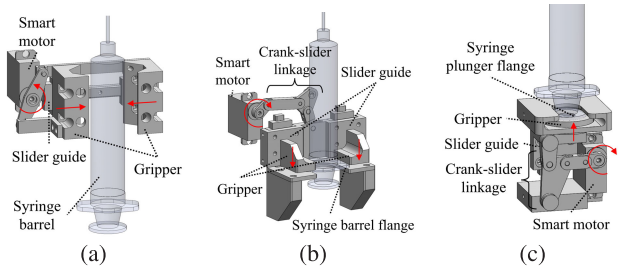

FIGURE 5. Structure of the syringe gripping mechanism. (a) Barrel. (b) Barrel flange. (c) Plunger flange.

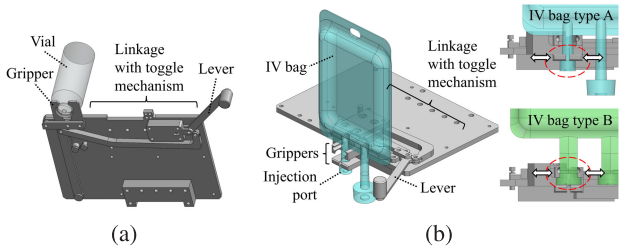

FIGURE 6. Structure of gripping mechanisms for medication containers. (a) Vial. (b) IV bag.

automatically hold 20–50 mL syringes while consistently aligning their center axis. In addition, the driving unit pushes or pulls the plunger linearly. The syringe is installed vertically, facing upward in the equipment. On the upper side of the syringe are manual gripping parts that allow easy installation of a vial and IV bag. The entire frame containing the vial gripper and the IV bag gripper is connected to a driving unit, enabling the upper frame to be translated up and down, and left and right.

The size of the equipment body alone, excluding the upper frame, is 184 mm wide, 125.5 mm deep, and 274 mm high, and is designed to be small enough to be placed and used in a general BSC. The equipment has a built-in rechargeable battery; therefore, it can operate without an external power supply. Its touch display allows users to intuitively monitor and control its operations.

1) AUTOMATIC SYRINGE GRIPPING MECHANISM

As shown in Fig. 5, the syringe gripping mechanism consists of a barrel centering gripper, barrel flange gripper, and plunger flange gripper [20]. Each actuation system for the three grippers was designed to be compact, using small, high output actuator modules of industrial specifications (MD89MW, HITEC).

The barrel-centering gripper (Fig. 5(a)) accurately aligns the central axis of the mounted syringe at a constant position, regardless of the diameter of the syringe barrel. The barrel gripper has inclined surfaces for centering and is moved using a crank-slider mechanism [21].

A large resistance force is exerted on the syringe when driving the plunger or when inserting the needle into the rubber stopper of the medicine container, which may cause the syringe barrel to slip on the gripper. A barrel flange gripper (Fig. 5(b)) was installed to solve this problem. The barrel flange gripper was designed based on a six-bar, crank-slider mechanism [22], allowing it to clamp the flange strongly.

The plunger flange gripper (Fig. 5(c)) was designed using the same mechanism as the barrel flange gripper.

2) MANUAL GRIPPING MECHANISMS FOR MEDICATION CONTAINERS

Manual gripping parts were developed to hold a vial and an IV bag firmly in a consistent position (Fig. 6 [20]).

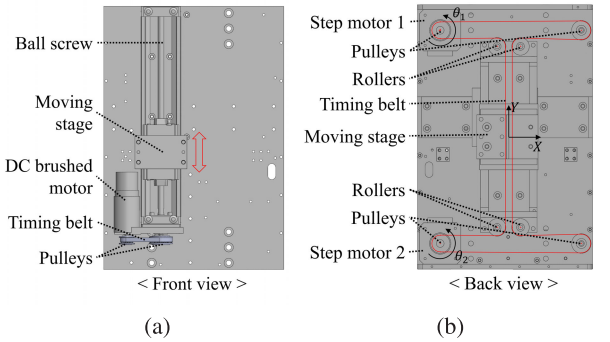

FIGURE 7. Driving mechanisms. (a) Syringe plunger drive. (b) Medication container transfer.

A toggle mechanism consisting of a linkage and preload spring was applied to each manual gripping part. Because of the toggle mechanism, users can easily open and close them with minimal effort.

The vial gripper features a circumferential surface designed to grip the bottle neck (Fig. 6(a)). There are two types of IV bag grippers (Types A and B in Fig. 6(b)), which are compatible with the various port shapes of IV bags. One is designed for small-diameter, cylinder-shaped ports, while the other is designed for large-diameter, polyhedron-shaped ports. Each IV bag gripper is opened and closed simultaneously, using a single mechanism.

3) DRIVING MECHANISMS FOR PLUNGER MANIPULATION AND TRANSLATION OF THE UPPER FRAME

The mechanism for pushing or pulling the syringe plunger (a type of linear actuator) includes a precision ball screw and timing belt pulleys (Fig. 7(a)). Its full stroke is 96 mm and covers the entire range of motion of the plunger in a 50 mL syringe (approximately 90 mm). A brushed DC motor with an output of 28 W (2642-024-CR, Faulhaber) was used in the linear actuator. At the rated speed of the selected motor (4370 r/min), the linear actuator can move the plunger at a speed of 40.5 mm/s. Additionally, under the condition of the selected motor's rated torque (0.032 N·m) and assuming 90% efficiency (the power transmission efficiency of the timing belt and ball screw), the linear actuator can drive the plunger with a force of 326 N.

When extracting water from a 50 mL vial filled with water using a 50 mL standard disposable syringe (barrel

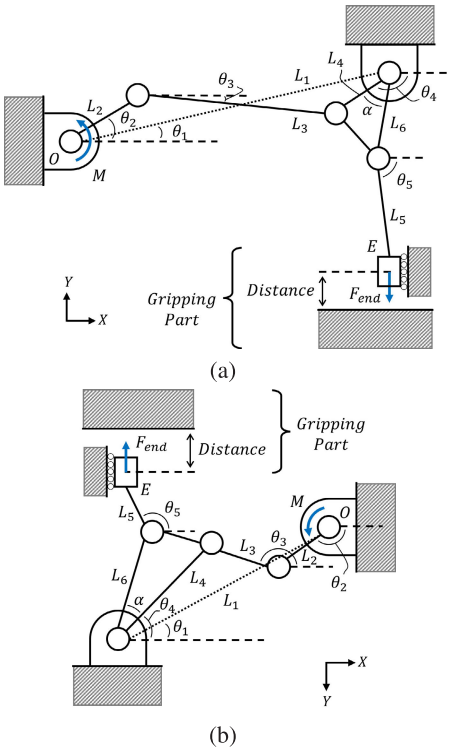

FIGURE 8. Kinematic diagram of the gripping mechanism of a syringe. (a) Barrel flange. (b) Plunger flange.

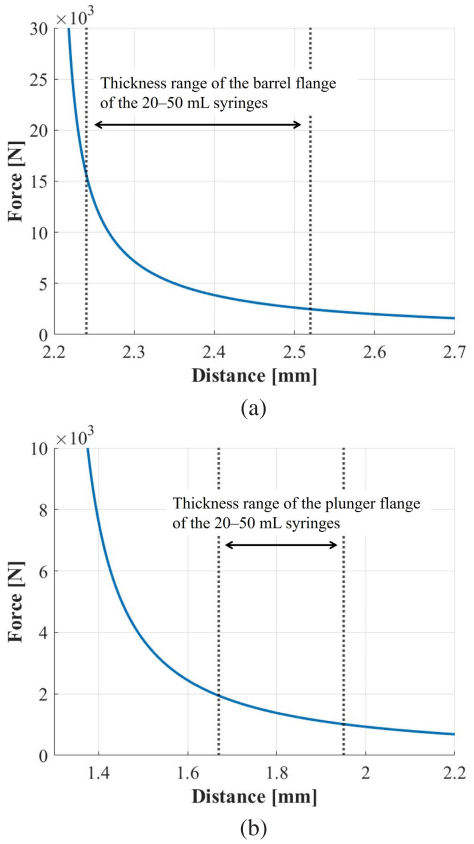

FIGURE 9. Force-distance curve of the gripping mechanism for a syringe. (a) Barrel flange. (b) Plunger flange.

internal diameter: 26.4 mm) with an 18 G needle at an average plunger speed of 4 mm/s (a general condition in manual compounding work), the force required to pull the plunger is approximately 50 N (this force was measured in a preliminary experiment; refer to the Appendix). Even though the plunger force may increase when dealing with drugs of higher viscosity, the driving mechanism has enough margin in both driving force and speed. This enough margin enhances equipment durability and long-term operation stability.

The driving mechanism for the upper frame, where a vial and IV bag are installed, is a type of 2-axis orthogonal transfer mechanism (Fig. 7(b)). This mechanism was designed based on an H-frame-type positioning system [23], [24]. Despite its compact size, it offers a substantial working range, with an X-axis stroke of 93 mm and a Y-axis stroke of 95 mm. This mechanism enables precise control over the relative positioning of the syringe and either the vial or IV bag, ensuring smooth insertion or removal of the syringe needle from the rubber stopper of the vial or IV bag. Furthermore, it effectively transports the drug solution from a vial to an IV bag using a syringe.

C. ANALYSIS OF KINEMATICS AND STATICS

1) SYRINGE GRIPPING MECHANISM

The following assumptions were made for kinematic and static analyses of the barrel/plunger flange grippers:

- All links are rigid elements that do not deform.
- The mass and volume of all links are ignored.
- All rotary joints are ideal pinned supports, and friction is ignored.
- The slider, which serves as the end effector, is an ideal roller support, and the friction is ignored.
- The system is in a quasi-static state, and all inertial forces are ignored.
- The driving torque applied to the crank is constant.

Figs. 8(a) and 8(b) show the structure and kinematic parameters of the gripper mechanisms of the barrel and plunger flanges, respectively. Point O is the center of the crank hinge and origin of the reference coordinate system. Point E is the center of the slider (end effector) and point of application of the gripping force. The slider moves vertically along the Y-axis, as shown in Fig. 8. Here, L_i denotes the length of the i-th link and θ_i represents the angle of the link with respect to the X-axis. α is the constant angle between the 4^{th} link (L_4) and the 6^{th} link (L_6). M is the crank driving torque at origin O; F_{end} is the gripping force applied at point E.

According to the kinematics of the four-bar linkage formed by the 2^{nd}, 3^{rd}, and 4^{th} links, the angle of the 3^{rd} link and the angle of the 4^{th} link can be determined for a given crank angle [21]. The X-axis position of point E is a fixed value, and the Y-axis position of point E can be calculated based on the kinematics of the 5^{th} and 6^{th} links (1). The gripper distance

can be calculated directly from the Y-axis position of point E.

$$E_y = L_1 \sin\theta_1 + L_6 \sin(\alpha + \theta_4) - \sqrt{(L_5)^2 - (B_1)^2} \quad (1)$$

where $B_1 = E_x - [L_1 \cos\theta_1 + L_6 \cos(\alpha + \theta_4)]$.

With the syringe clamped in the gripper, the gripping force (F_{end}) is determined based on the force and moment equilibrium equations of all links and slider elements:

$$F_{end} = \frac{L_4(\tan\theta_3 \cos\theta_4 + \sin\theta_4)}{L_6\,[\cos(\alpha + \theta_4) + \sin(\alpha + \theta_4)\cot\theta_5]} B_2 \quad (2)$$

where

$$B_2 = \frac{M}{L_2(\tan\theta_3 \cos\theta_2 + \sin\theta_2)}.$$

Fig. 9 shows how the gripping force applied to the barrel/plunger flange changes depending on the gripper distance. The gripping force was calculated under the condition of half of the motor's stall torque (3.2 kgf·cm). The average thickness of the barrel flange and plunger flange of the 20–50 mL syringes was 2.28 mm and 1.81 mm, respectively, and the dimensional deviation was ±0.14 mm. The areas bounded by the dotted lines in Figs. 9(a) and 9(b) represent the thickness ranges. Based on the static analysis, the barrel flange gripper can apply a gripping force of at least 2400 N (Fig. 9(a)), whereas the plunger flange gripper can exert a gripping force of at least 1000 N (Fig. 9(b)).

Using the proposed gripper mechanism, the syringe flange can be securely fixed, even with thickness deviations. When the flange is clamped by the gripper, the linkage mechanism approaches its kinematic singular position, and the transmission ratio between the motor's driving torque and gripping force increases exponentially. Consequently, a sufficiently strong gripping force can be generated without increasing the motor torque output.

2) MANUAL GRIPPING MECHANISMS FOR MEDICATION CONTAINERS

Figs. 10(a) and 10(b) show the structure and kinematic parameters of the gripping mechanisms for a vial gripper and IV bag gripper, respectively. Here, L_i denotes the length of the i-th link and θ_i represents the angle of the link with respect to the X-axis. β is the constant angle between the 1st link (L_1) and the 2nd link (L_2). F_{in} is the driving force applied to the lever end perpendicular to the 1st link.

Point C is the center of the pin connection between the lever and slider, as well as where the restoring force (f_c) from the preload spring is applied. The slider moves horizontally along the X-axis, as shown in Fig. 10. Immediately before the drug container (vial or IV bag) contacts the gripper, point C maintains its mechanical limit position owing to the restoring force. Unless an external force is applied that surpasses the spring force, point C remains stationary. In this case, the position of a gripper end (point E) for a given lever angle can be calculated using the kinematics of the four-bar linkage comprising the 2nd, 3rd, and 4th links.

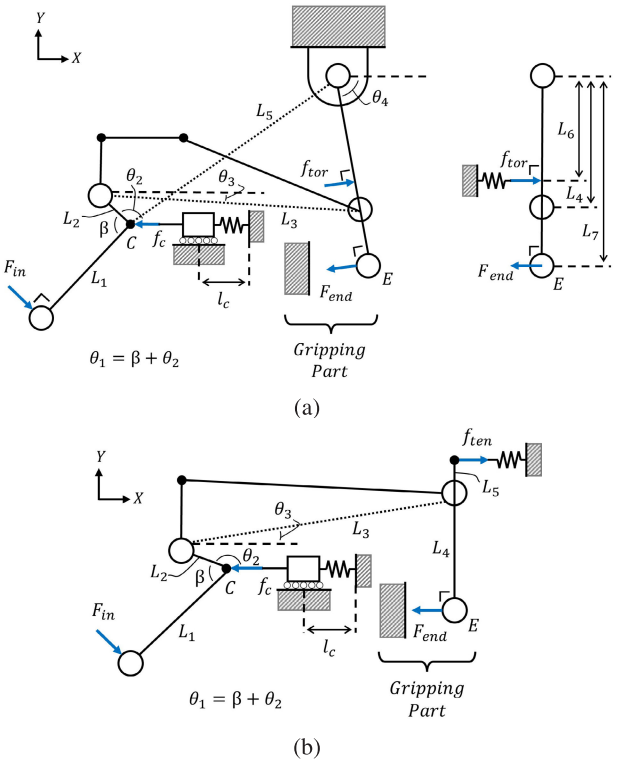

FIGURE 10. Kinematic diagram of the gripping mechanism for medication containers. (a) Vial. (b) IV bag.

X-axis position of point E with respect to point C in case of vial gripper:

$$E_{x,vial} = L_2 \cos\theta_2 + L_3 \cos\theta_3 + (L_7 - L_4)\cos\theta_4 \quad (3)$$

X-axis position of point E with respect to point C for IV bag gripper:

$$E_{x,bag} = L_2 \cos\theta_2 + L_3 \cos\theta_3 \quad (4)$$

After the drug container (vial or IV bag) is gripped, the end of the gripper (point E) becomes stationary. Subsequently, the position of the 4th link remains fixed, whereas point C translates according to the lever angle changes. Consequently, the preload spring connected to point C becomes more compressed. The position of point C for a given lever angle can be determined based on the kinematics of the crank-slider mechanism, involving the 2nd and 3rd links.

Compression distance of the preload spring in the case of the vial gripper:

$$l_{c,vial} = E_{x,vial} - (L_7 - L_4)\cos\theta_4 - (L_2 \cos\theta_2 + L_3 \cos\theta_3) + l_{init,vial} \quad (5)$$

Compression distance of the preload spring in the case of the IV bag gripper:

$$l_{c,bag} = E_{x,bag} - (L_2 \cos\theta_2 + L_3 \cos\theta_3) + l_{init,bag} \quad (6)$$

The proposed gripper mechanism has an auxiliary spring that facilitates the easy opening of the gripper (torsion spring

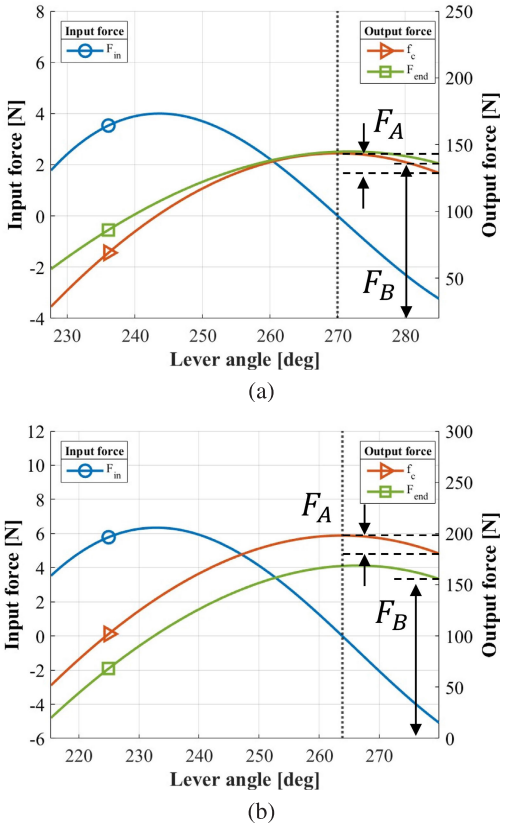

FIGURE 11. Force curve of the gripping mechanism for medication containers. The dotted vertical line perpendicular to the X-axis indicates when the restoring force of the preload spring (f_c) reaches its maximum. (a) Vial. (b) IV bag.

for the vial gripper and tension spring for the IV bag gripper), and the direction of the auxiliary spring force is assumed to be perpendicular to the 4th link (f_{tor} in Fig. 10(a) and f_{ten} in Fig. 10(b)).

If the gripper mechanism remains in a quasi-static state, the force and moment equilibrium equations for all links can be derived for a given lever angle. From these equations, the major forces can be determined as follows:

The lever driving force in the case of both grippers:

$$F_{in} = \frac{L_2(\tan\theta_3\cos\theta_2 - \sin\theta_2)}{L_1 + L_2\sin\theta_1(\tan\theta_3\cos\theta_2 - \sin\theta_2)} f_c \quad (7)$$

The gripping force in the case of the vial gripper:

$$F_{end,vial} = \frac{L_6 f_{tor} - B_3 L_4(\tan\theta_3\cos\theta_4 + \sin\theta_4)}{L_7} \quad (8)$$

where $B_3 = f_{c,vial} + F_{in,vial}\sin\theta_1$.

The gripping force in the case of the IV bag gripper:

$$F_{end,bag} = f_{c,bag} + F_{in,bag}\sin\theta_1 - f_{ten} \quad (9)$$

Fig. 11(a) illustrates the three major forces calculated for the vial gripper, which clamps a vial with a bottleneck diameter of 16.4 mm. Fig. 11(b) shows the forces calculated for the IV bag gripper, which clamps an IV bag with an injection port width of 8.7 mm.

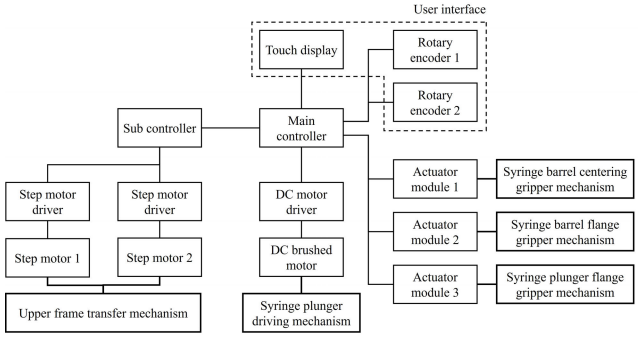

FIGURE 12. Components and structure of the control system.

Upon contact with the medicine container (vial or IV bag), the continuous rotation of the lever in the closing direction leads to the further compression of the preload spring. This results in an increased restoring force and stronger gripping force exerted on the drug container. After the magnitude of the preload spring force exceeds its maximum value, the lever reaches a mechanical limit position. The preload spring force ensures that the lever remains at its mechanical limit position, preventing it from returning to its starting position. Consequently, the gripper can remain closed and securely hold the medication container in place. The magnitude of the gripping force applied to the drug container corresponds to the F_B shown in Figs. 11(a) and 11(b) (vial gripper: approximately 136 N; IV bag gripper: approximately 156 N).

To separate the medicine container from the gripper, an additional force must be applied to the preload spring, and the magnitude of the additional force (F_A shown in Figs. 11(a) and 11(b)) is significantly lower than that of the gripping force F_B (vial gripper: approximately 15 N; IV bag gripper: approximately 18 N). Moreover, the gripper can be easily opened using a lever, which requires less force than F_A because of the principle of leverage.

D. DESIGNING THE CONTROL SYSTEM

Fig. 12 shows the components and structure of the control system. The main controller processes the syringe gripping mechanism, plunger drive actuator, and user interfaces, such as a touch display. The subcontroller, under the main controller's direction, controls the transporting mechanism for the upper frame, which holds the medicine containers (a vial and an IV bag). The main controller identifies the size of the syringe installed, calculates the plunger moving distance for a predetermined medication dose, and then drives the plunger to extract the drug solution. At the beginning of the extraction process, the main controller pulls and pushes the plunger a small distance to eliminate any air trapped in the syringe barrel and needle, thereby reducing errors in the quantity of drug extraction. Considering that the plunger speed affects the air bubble generation within the syringe, the hydrodynamic phenomenon inside the syringe was simulated to determine the appropriate plunger speed. Further details on this matter are provided in Section II-E.

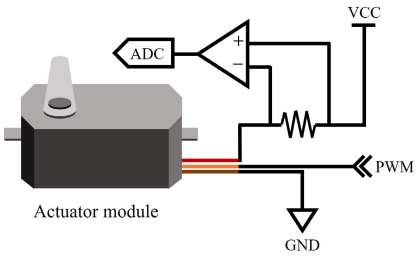

FIGURE 13. Current sensing circuit for the actuator module.

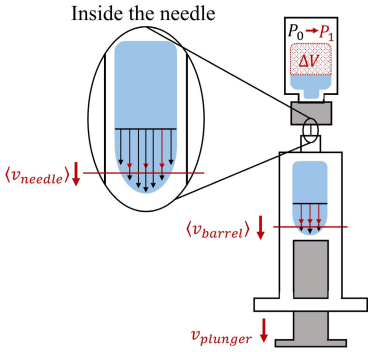

FIGURE 14. Fluid flow and pressure drop within a vial, syringe needle, and syringe barrel during the process of fluid extraction using a syringe.

If an object other than a standard syringe is inserted into the syringe grippers, or if a syringe is placed excessively off-centered, an unusual force may be applied to the grippers. In this case, a large current flows continuously to the gripper motors, which may cause a motor breakdown. As the actuator module does not output a current-sensing signal, there is no way to measure the current flowing through the internal motor wire [25]. In this study, a precise shunt resistor and differential amplifier were integrated into the power input lines of the actuator module, as illustrated in Fig. 13, enabling the measurement of the current supplied to the actuator module. Because the actuator module is internally controlled by a switching drive, its power-side current is not equivalent to the current flowing through the motor coil most of the time. However, a continuous large current is usually induced when the actuator module does not move at an unusual position. In this case, the power-side current can be used as an alternative signal for the current flowing through the motor wire, because the two signals have a positive correlation, even though the power-side current is smaller than the motor current. When the power-side current of the actuator module exceeds a preset upper limit, the main controller adjusts the motor's position command to prevent further increase. This helps the motor to relieve itself from overload, resulting in a decrease in current.

The other purpose of the proposed current-sensing and overcurrent-limiting method is to monitor the installed state of a syringe. If the motor current increases when the motor position is outside the expected syringe barrel diameter range (based on the user-entered syringe size via the touch display), the main controller interprets this situation as either the syringe is not properly aligned in the gripper or the installed syringe size differs from what the user has entered. In this case, the main controller does not proceed to the next step but displays a warning message to prompt the user to check the syringe installation status.

E. SPEED PROFILE DESIGN CONSIDERING CAVITATION OCCURRENCE

The presence of air bubbles in the syringe during medication extraction can lead to errors in the extracted amount, which is an important issue to address. During manual compounding, pharmacists attempt to remove air bubbles by shaking the syringe or pushing the plunger while holding the needle vertically upward. However, it is challenging to completely remove small bubbles using these methods. Therefore, it is important to carefully draw the drug solution from the vial to minimize the generation of air bubbles.

Air bubbles can be generated inside a syringe through cavitation [26], [27], [28], [29]. During drug extraction, negative pressure builds up within the vial; in the absence of air ventilation, this negative pressure intensifies as the drug is extracted. When the pressure of the drug solution in the syringe falls below its vapor pressure, the solution vaporizes (cavitation). The fluid pressure loss is directly related to the average fluid velocity. Therefore, if the syringe plunger is operated slowly, fewer air bubbles are generated inside the syringe. However, a lower plunger driving speed also reduces dispensing efficiency.

To optimize the plunger driving speed, the hydrodynamic phenomenon of syringe operation was modeled and simulated. Using this model, a speed profile for plunger driving was designed. In the simulation, the fluid inside the vial and syringe was assumed to be pure water, at room temperature (25°C). The geometry and configuration of the vial, needle, and syringe are shown in Fig. 14. The syringe was aligned vertically upward, and the vial, needle, and syringe had perfectly axisymmetric cylindrical shapes with a consistent diameter along their length. Fluid leakage or air inflow into the fluid channel (vial-needle-syringe), as well as pressure due to the mass of the fluid column in the channel, were ignored. If the air inside the vial behaves as an ideal gas, according to Boyle's law, the change in the air pressure inside the vial can be calculated based on the change in the volume of the air layer inside the vial, which is equivalent to the change in the volume of the fluid inside the vial.

$$P_0 V_0 = P_1 V_1 \tag{10}$$

$$P_1 = P_0 \frac{V_0}{V_1} = P_0 \frac{V_0}{V_0 + \Delta V} \tag{11}$$

$$\Delta P = P_0 - P_1 = P_0 \frac{\Delta V}{V_0 + \Delta V} \tag{12}$$

P_0 and V_0 represent the initial air pressure and fluid volume in the vial, respectively, and P_1 and V_1 denote the air pressure and fluid volume after fluid extraction, respectively. In this

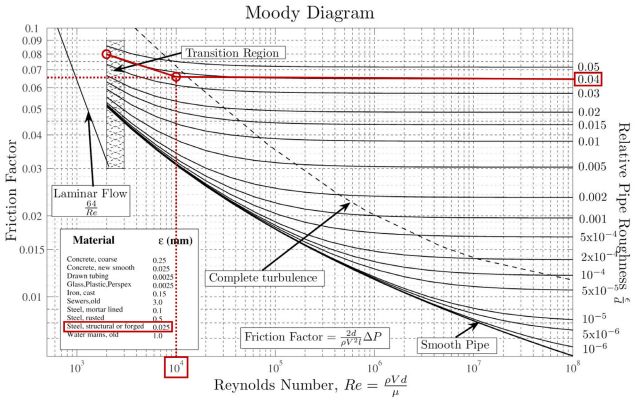

FIGURE 15. Moody diagram (reproduced from [30]).

study, the initial air pressure inside the vial was set to be equal to the atmospheric pressure ($P_0 = P_{atm}$).

The change in the fluid volume inside the vial can be calculated from the flow rate at the needle:

$$\Delta V = A_{needle}\langle v_{needle}\rangle \Delta t \tag{13}$$

where $\langle v_{needle}\rangle$ means the average value of the variable v_{needle}.

According to the continuity equation, the flow rates in the needle and barrel are equal:

$$A_{barrel}\langle v_{barrel}\rangle = A_{needle}\langle v_{needle}\rangle \tag{14}$$

The average fluid velocity in the syringe barrel is assumed to be equal to the driving speed of the plunger:

$$\langle v_{barrel}\rangle = v_{plunger} \tag{15}$$

The pressure loss in a pipe with constant cross-sectional area is described by the Darcy–Weisbach equation:

$$P_{loss} = f_D \cdot \frac{\rho L}{2} \cdot \frac{\langle v\rangle^2}{D} \tag{16}$$

where f_D is the Darcy friction factor; ρ is the mass density of the fluid; L and D are the length and diameter of the pipe, respectively; and $\langle v\rangle$ denotes the average fluid velocity in the pipe.

The Darcy friction factor is a function of the Reynolds number of the fluid and the relative pipe roughness of the pipe, which can be obtained by referring to the Moody diagram (Fig. 15 [30]). The Reynolds number is the ratio of the inertial force to the viscous force of the fluid and is a dimensionless number related to viscosity and average fluid velocity:

$$Re = \frac{\langle v\rangle D}{\nu} \tag{17}$$

where ν is the kinematic viscosity of the fluid, and the kinematic viscosity of water at room temperature (25°C) is 0.8928 mm^2/s [31].

When the fluid passes through the needle, the cross-sectional area is the smallest, and the fluid velocity is the fastest, making the pressure loss at the needle dominant.

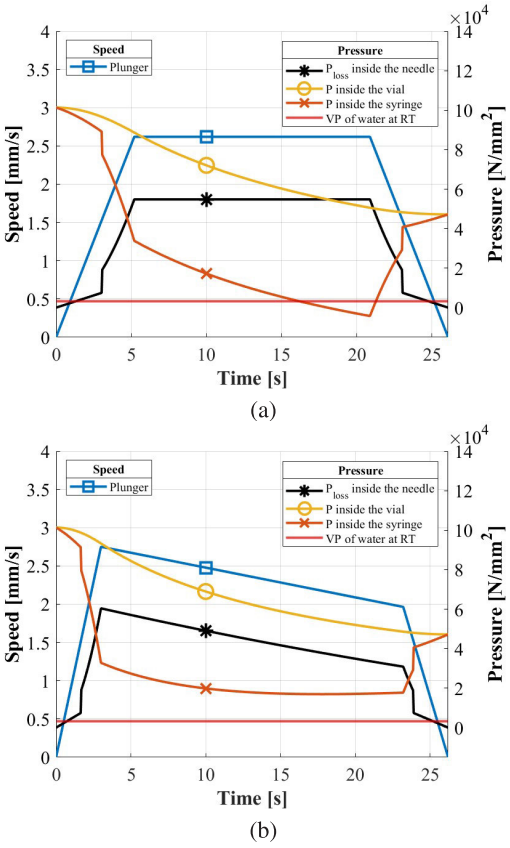

FIGURE 16. Simulation results: Pressure change according to plunger speed profile. (a) Standard trapezoidal profile. (b) Modified trapezoidal profile.

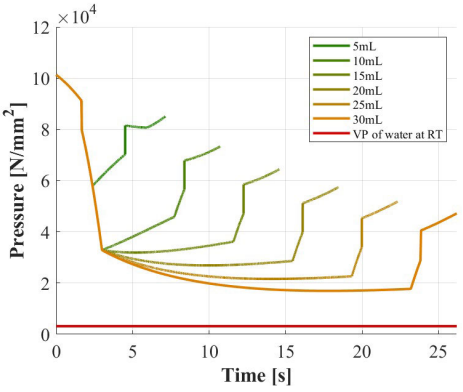

FIGURE 17. Simulation results: Pressure change according to target medication extraction volume.

Therefore, the pressure loss inside the vial and syringe barrel was ignored. To calculate the pressure loss at the needle, it is necessary to first determine the friction factor of the needle. If the Reynolds number is less than 2000, the fluid flow corresponds to laminar flow, and the friction factor is determined only by the Reynolds number. However, when the Reynolds number exceeds 2000, the fluid flow transitions to turbulent flow, and the trend of the friction factor changes depending on the relative roughness of the pipe.

In this study, the needle material was assumed to be structured steel (harsh condition) with an average roughness

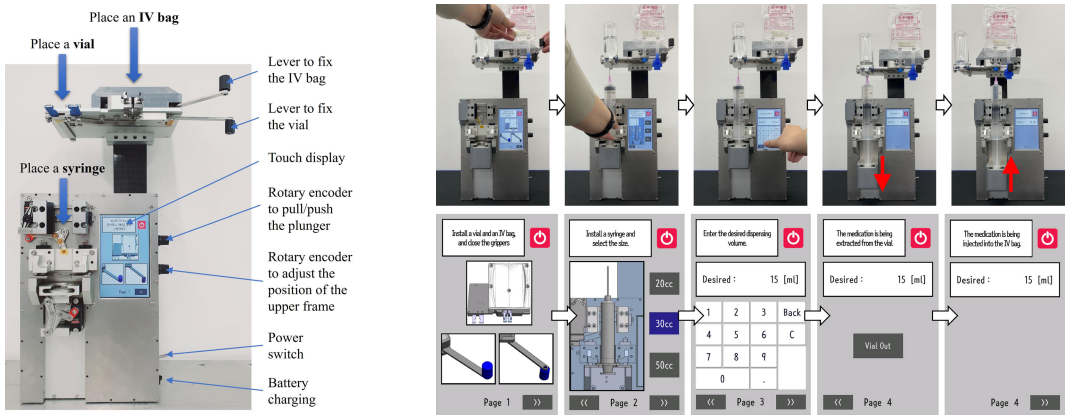

FIGURE 18. Prototype and its working sequence.

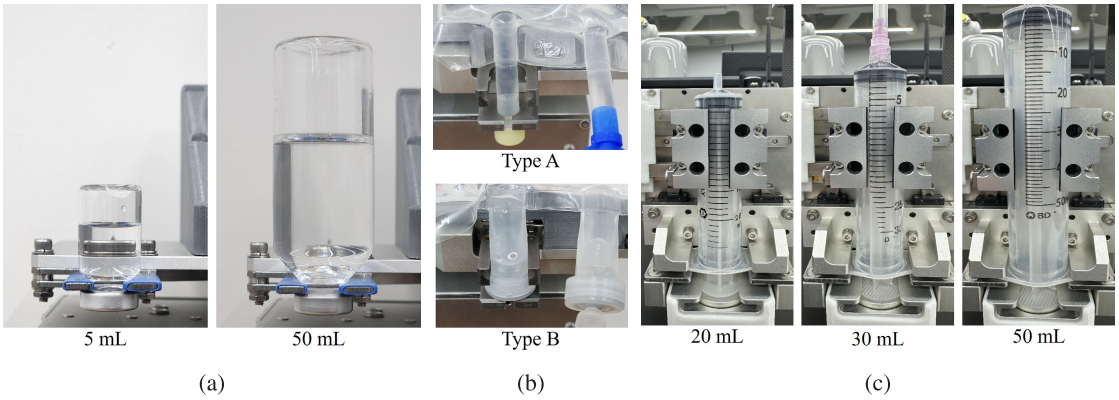

FIGURE 19. Compatibility with various vials, IV bags, and syringes.

(ϵ) of approximately 0.025 mm, as indicated in the Moody diagram. The needle size was specified as 18 G, with an inner diameter of approximately 0.6 mm. Subsequently, the relative pipe roughness was calculated as approximately 0.04. For easy calculations, the friction factor curve in the turbulent flow region was simplified, as depicted by the red line in Fig. 15:

$$f_D = \begin{cases} \dfrac{64}{Re}, & (0 < Re < a_1) \\ -k \cdot Re + 0.08, & (a_1 \le Re < a_2) \\ 0.065, & (Re > a_2) \end{cases} \tag{18}$$

where $a_1 = 2 \times 10^3$, $a_2 = 10^4$, and $k = 1.53 \times 10^{-7}$.

In the simulation, the change in fluid pressure inside the syringe barrel was estimated according to (10)-(18) for a given plunger speed profile at each time step, and then the estimated value was compared with the water vapor pressure ($P_{vapor} = 3169$ N/m^2 at 25°C) to determine whether cavitation occurred.

$$P_{barrel} = \Delta P_{vial} - P_{loss} < P_{vapor} \tag{19}$$

The simulation conditions were set to extract 30 mL of water using a 50 mL vial, syringe, and 18 G needle, with the initial volume of water inside the vial set at 35 mL. Figs. 16(a) and 16(b) compare the standard trapezoidal profile with the modified profile and resulting pressure change. The average flow rates in both cases were similar, and the total extraction time was approximately 26 s.

As shown in Fig. 16(a), cavitation is predicted to occur after approximately 16 s when the plunger is driven according to the standard trapezoidal profile. On the other hand, as shown in Fig. 16(b), when the plunger is driven according to the modified profile, the fluid pressure inside the syringe barrel did not decrease below the vapor pressure. This indicates that cavitation did not occur.

The target quantity for fluid extraction can be adjusted by tuning the duration of the middle section of the modified profile or by scaling the maximum speed. However, cavitation did not occur regardless of the extraction volume, as shown in Fig. 17.

III. RESULTS

A. PROTOTYPE AND CALIBRATION

Fig. 18(a) shows the prototype developed in this study. Fig. 18(b) illustrates the operational sequence of extracting the drug from a vial and moving the upper frame to deliver the drug into an IV bag. The equipment was designed to

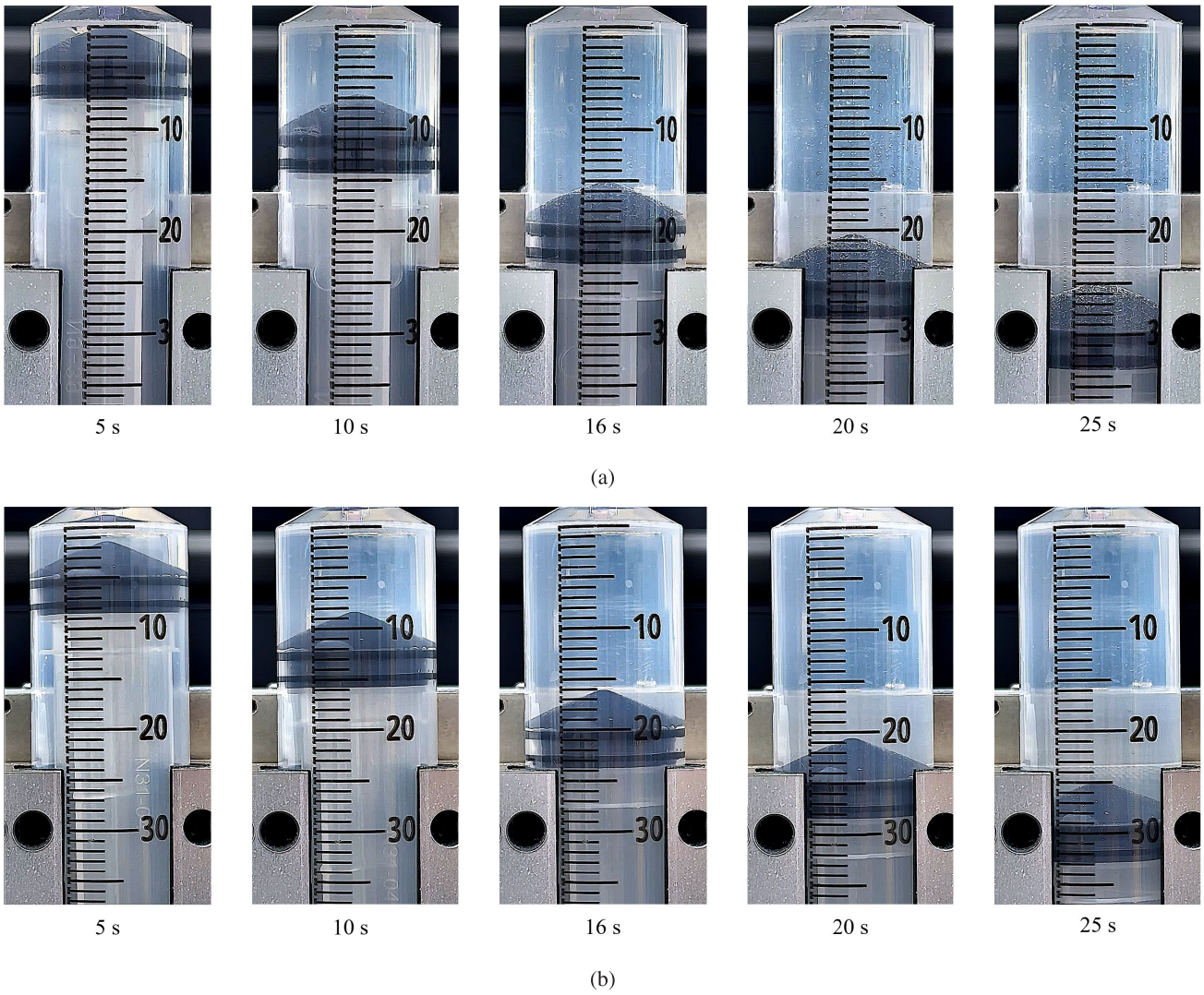

FIGURE 20. Experimental results. (a) Standard trapezoidal profile. (b) Modified trapezoidal profile.

be compatible with standard vials, IV bags, and syringes of various capacities, as shown in Fig. 19.

The working sequence of the equipment involves five steps: 1) place the vial and IV bag, 2) place the syringe, 3) enter the target dispensing volume, 4) extract the drug from the vial, and 5) transfer and inject the drug. Only steps 1–3 require user intervention, whereas the equipment automatically executes steps 4 and 5. Since users only place a syringe in the gripping mechanism during the initial preparation step, exposure to the drug is significantly minimized, and needlestick accidents can be reduced, ensuring the safety of medication compounding. User guidance messages are displayed on the front panel (Fig. 18(b)) for each step, making it easy to understand how to operate the equipment. This interface is user-friendly and intuitive; therefore, a minimal training period and cost are required.

When using this equipment to compound multiple medications in a single IV bag, it is crucial to prevent mixing the drug solutions inside the vials. Thus, users should replace the syringe and needle with new ones each time they switch medication vials containing a pure drug solution.

The driving stroke of the syringe plunger, which corresponds to the intended quantity, can be estimated from the internal cross-sectional area of the syringe barrel and density of the solution. Nevertheless, to enhance accuracy, the plunger driving stroke can be calibrated.

Two variables can be used as references for calibration: the amount of extraction from a vial and the amount injected into an IV bag. The former refers to the vial weight difference before and after extracting the drug solution with a syringe, whereas the latter refers to the IV bag weight difference before and after injecting the drug solution with a syringe. The latter is an inaccurate measure for evaluating the dispensing accuracy. This is due to the expansion of the volume of the IV bag upon injection of the drug solution, which results in an increase in the air buoyancy exerted on the IV bag. Consequently, the weight difference of the IV bag is smaller than the actual weight difference [32], [33], [34].

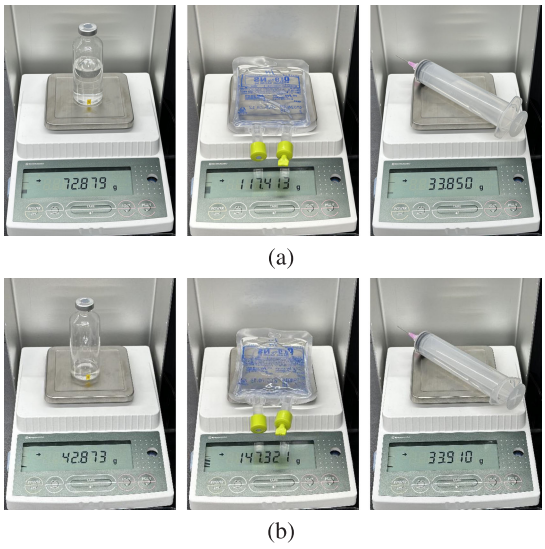

FIGURE 21. Experimental results. (a) Before extraction. (b) After injection.

On the other hand, in the case of vials, if the opening remains sealed with a rubber stopper and aluminum cap, there is no change in volume before and after solution extraction; therefore, there is no change in air buoyancy on the vial. In other words, the change in the weight of the entire vial exactly matches the weight of the extracted drug solution. Therefore, in this study, the driving stroke of the syringe plunger was calibrated by referring to the amount extracted from a vial. The performance of the calibrated equipment was experimentally verified (Section III-C).

B. EVALUATION OF CAVITATION OCCURRENCE UNDER DIFFERENT SPEED PROFILES

In this section, we experimentally evaluate the occurrence of cavitation during syringe plunger manipulation. The experimental conditions were identical to the simulation conditions described in Section II-E. When the plunger was controlled using a standard trapezoidal speed profile, large bubbles were generated inside the barrel at approximately 16 s, as predicted by the simulation (Fig. 20(a)). On the other hand, when the plunger was controlled using the modified profile, almost no bubbles were generated inside the barrel, as predicted in the simulation (Fig. 20(b)).

The experimental results, confirmed that the simulation model proposed in this study well reflects the actual physical phenomenon of extracting a drug solution with a syringe, and can predict the occurrence of cavitation inside the syringe. In addition, it was verified that applying the proposed speed profile could reduce the generation of bubbles owing to cavitation.

C. EVALUATION OF MEDICATION DISPENSING ACCURACY

To evaluate the compounding accuracy of the developed equipment, experiments were conducted according to the following procedures:

TABLE 1. Experimental results of dispensing medication (50 mL syringe).

[Unit: g]	Change in mass = (| Initial mass - final mass |)		
	A	B	
	Vial	IV bag	Syringe
1	30.026	29.937	0.054
2	29.976	29.881	0.059
3	30.006	29.882	0.086
4	29.975	29.903	0.040
5	30.015	29.901	0.080
6	**30.006**	**29.908**	**0.060**
7	29.975	29.905	0.037
8	30.015	29.915	0.061
9	30.022	29.891	0.086
10	29.973	29.899	0.047
Mean value	**29.999**	29.902	0.061
Maximum value	**30.026**	29.937	0.086
Minimum value	**29.973**	29.881	0.037
Standard deviation	**0.021**	0.016	0.017

TABLE 2. Comparison of accuracy and precision between robotic and manual compounding.

Geersing, T. H., et al. 2020 [36]				
	Robotic compounding		Manual compounding	
Material	MTX[1]	CPA[2]	MTX	CPA
Accuracy (mean absolute dose error)	0.25 mg (0.5%)	-8.09 mg (-0.67%)	-0.98 mg (-1.96%)	2.16 mg (0.18%)
Precision (standard error)	0.44 mg	1.80 mg	0.33 mg	3.36 mg
Iwamoto, Takuya, et al. 2017 [37]				
	Robotic compounding		Manual compounding	
Material	FU[3]	CPA	FU	CPA
Accuracy (mean absolute dose error)	0.83%	0.52%	1.20%	1.70%
Precision (coefficient of variation)	1.04%	0.59%	1.46%	2.20%

[1] Methotrexate
[2] Cyclophosphamide
[3] Fluorouracil

(1) Prepare a 50 mL vial, an IV bag, and a 50 mL standard disposable syringe equipped with an 18 G needle.
(2) Inject 35 mL of room temperature water into the vial and seal it with a rubber stopper and aluminum cap.
(3) Measure the initial weights of the prepared vial, IV bag, and syringe, and then install them onto the developed equipment.
(4) Using this equipment, extract 30 g of water from the vial and inject it into the IV bag.

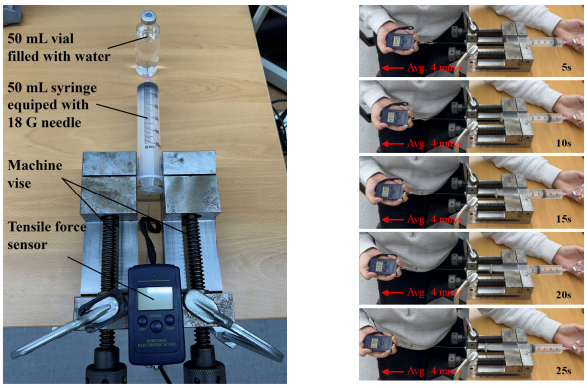

(a) (b)

FIGURE 22. Preliminary experiment to measure the plunger driving force. (a) Experimental setup. (b) Experimental sequence.

(5) Measure the final weights of the vial, IV bag, and syringe after the water extraction and injection processes.
(6) Repeat the above process.

Fig. 21 shows the weight measurement results of the 6th experiment. The minimum unit of the scale used for weight measurement (BL320H, SHIMADZU) was 0.001 g, and its linearity was ±0.003 g. Table 1 summarizes the results of 10 repeated experiments. When examining the dose extracted from the vial in Table 1, the maximum error compared to the target dosage (30 g) was 27 mg, and the peak-to-peak error range of the extracted amount was within ±0.09% of the target quantity. This represents very high accuracy compared with the tolerance range of medication compounding specified in international standards (±5% [2], [35]). The average change in syringe weight was only 61 mg, indicating that only a minimal amount of medication remained.

When comparing the weight change of the vial (value A in Table 1) with the sum of the weight change of the IV bag and syringe (value B in Table 1), the latter (B) was, on average, 36 mg less than the former (A). The volume change in the IV bag corresponded to the volume of the injected water (approximately 30 mL). Considering the air density (1.184 kg/m^3 at 25°C), the weight of the air displaced by this volume change was approximately 35.5 mg. Therefore, the observed weight difference of 36 mg can be attributed to the volume change in the IV bag and resulting air buoyancy, as discussed in Section III-A.

IV. DISCUSSION

The experimental results showed that the developed equipment could accurately extract water from a vial according to the prescribed dosage and inject it into an IV bag. Additionally, the low standard deviation indicates that the operation of the developed equipment is highly repeatable.

Several studies have compared the performance of commercial anticancer drug compounding robots (APOTECAchemo, Loccioni) and manual compounding (Table 2, [36], [37]); in the case of robotic compounding, the mean absolute dose error is less than 1% of the target quantity, while the accuracy of manual compounding exceeds 1%. Comparing the findings from the referenced studies with the experimental results of this study, it is evident that the developed equipment performs with comparable accuracy to more expensive and complex robotic compounding systems.

The developed equipment effectively minimized the residual water in the syringe during the extraction and injection processes. As described in Section III-A, the plunger driving stroke was calibrated based on the vial extraction weight. However, adjusting the calibration to consider the small residual amount in the syringe can enhance the accuracy of matching the actual amount injected into the IV bag with the target dispensing amount.

The time required for one cycle from extraction to injection was approximately one minute, which may have been longer than when a skilled pharmacist manually compounded the drug. However, using the developed equipment, the same work can be repeated with consistent accuracy and speed, increasing the productivity compared to manual methods.

The kinematic viscosity ν of medication influences cavitation conditions. Adjustment to the speed profile may be necessary if a drug solution other than water is used. If experimental data on various drugs are accumulated, the developed equipment can effectively operate under the optimized conditions for each drug.

V. CONCLUSION

In this study, we developed practical equipment to automate syringe manipulation to enhance medication-compounding processes. The newly developed machine was compactly designed to be placed within a typical biological safety cabinet workspace and was compatible with 20–50 mL disposable syringes, various types of vials, and IV bags. The process of drug extraction and injection is automated and only requires syringes and needles as consumables.

The speed profile was optimized and implemented to minimize cavitation inside the syringe during drug extraction, thereby reducing the work time and improving the dispensing accuracy. The experimental results demonstrate that the developed equipment achieves a high dispensing accuracy and repeatability (error range: ±0.09%, standard deviation: 21 mg). Additionally, residual amounts in the syringe were minimized during the extraction and injection processes.

Compared to commercial robotic compounding systems, this equipment has a simpler structure and is cost-effective while achieving performance levels comparable to those of robotic systems. This equipment can be invaluable in sterile compounding facilities that handle hazardous drugs, such as anticancer medications, and can serve as an affordable alternative to robotic systems.

APPENDIX

We measured the force required to pull the plunger in a preliminary experiment (Fig. 22(a)). Water was extracted from a 50 mL vial at a plunger speed of 4 mm/s using a standard 50 mL disposable syringe with an 18 G needle. A tensile force sensor was installed directly on the plunger. The results showed an average force of 50 N to pull the plunger, with some variations observed (Fig. 22(b)).

REFERENCES

[1] Food U. Drug Administration (FDA). (Jun. 29, 2022). *Compounding and the FDA: Q & A*. Accessed: Apr. 2, 2024. [Online]. Available: https://www.fda.gov/drugs/human-drug-compounding/compounding-and-fda-questions-and-answers

[2] L. B. Poppe, S. W. Savage, and S. F. Eckel, "Assessment of final product dosing accuracy when using volumetric technique in the preparation of chemotherapy," *J. Oncol. Pharmacy Pract.*, vol. 22, no. 1, pp. 3–9, Feb. 2016.

[3] X. Feng, K.-W. Wu, V. Balajee, J. Leissa, M. Ashraf, and X. Xu, "Understanding syringeability and injectability of high molecular weight PEO solution through time-dependent force-distance profiles," *Int. J. Pharmaceutics*, vol. 631, Jan. 2023, Art. no. 122486.

[4] V. MacDonald and P. J. Keir, "Assessment of musculoskeletal disorder risk with hand and syringe use in chemotherapy nurses and pharmacy assistants," *IISE Trans. Occupational Ergonom. Human Factors*, vol. 6, nos. 3–4, pp. 128–142, Oct. 2018.

[5] *Syringe Pump HK-400*. Accessed: Apr. 2, 2024. [Online]. Available: https://infinita-medical.eu/en/vet-equipment/250-syringe-pump-hk-400.html

[6] (Dec. 2012). *New Noteworthy—Pharmacy Purchasing Products Magazine*. Accessed: Apr. 2, 2024. [Online]. Available: https://www.pppmag.com/new_noteworthy/?noteid=659

[7] MSB. (2015). *Delivery, Installation and Commissioning of the First Robotic System for Cytostatic IV Solutions in Bulgaria*. Accessed: Apr. 2, 2024. [Online]. Available: https://www.msb.bg/en/projects/

[8] V. Surya, S. Bose, S. Kulkarni, and K. D, "Ocular drug delivery system using open-source syringe pump," *Asian J. Pharmaceutical Clin. Res.*, vol. 11, no. 6, pp. 152–157, Jun. 2018.

[9] J. Ulbrich, R. Swader, G. Petry, B. L. Cox, R. L. Greene, K. W. Eliceiri, and R. G. Radwin, "A syringe adapter for reduced muscular strain and fatigue," *Appl. Ergonom.*, vol. 85, May 2020, Art. no. 103061.

[10] K. S. Tee, M. S. Saripan, H. Y. Yap, and C. F. Soon, "Development of a mechatronic syringe pump to control fluid flow in a microfluidic device based on polyimide film," *IOP Conf. Ser., Mater. Sci. Eng.*, vol. 226, Aug. 2017, Art. no. 012031.

[11] M. I. Ali, "Designing a low-cost and portable infusion pump," in *Proc. 4th Int. Conf. Emerg. Trends Eng., Sci. Technol. (ICEEST)*, Dec. 2019, pp. 1–4.

[12] H. Kim, D. Cheon, J. Lim, and K. Nam, "Robust flow control of a syringe pump based on dual-loop disturbance observers," *IEEE Access*, vol. 7, pp. 135427–135438, 2019.

[13] M. F. M. Mazlan, S. Z. Salleh, M. S. A. Karim, and N. A. A. Razak, "Design and development of automated dispensing machine as medical device-based application: A review," *Proc. Inst. Mech. Eng. C, J. Mech. Eng. Sci.*, vol. 236, no. 18, pp. 10033–10050, Sep. 2022.

[14] L. Soumoy and J.-D. Hecq, "Automated compounding of intravenous therapy in European countries: A review in 2019," *Pharmaceutical Technol. Hospital Pharmacy*, vol. 4, no. 2, pp. 51–57, Aug. 2019.

[15] G. Nam, Y. J. Kim, Y. J. Kim, Y. J. Kim, J. A. Seo, K. Kim, and K. G. Kim, "Development of dual-arm anticancer drug compounding robot and preparation system with adaptability and high-speed," *J. Int. Soc. Simul. Surg.*, vol. 3, no. 2, pp. 64–68, Dec. 2016.

[16] S. Shin, J. Koo, S. W. Kim, S. Kim, S. Y. Hong, and E. Lee, "Evaluation of robotic systems on cytotoxic drug preparation: A systematic review and meta-analysis," *Medicina*, vol. 59, no. 3, p. 431, Feb. 2023.

[17] W.-H. Chen, L.-J. Shen, R.-J. Guan, and F.-L. L. Wu, "Assessment of an automatic robotic arm for dispensing of chemotherapy in a 2500-bed medical center," *J. Formosan Med. Assoc.*, vol. 112, no. 4, pp. 193–200, Apr. 2013.

[18] H. Jin, P. Gao, J. Cao, Y. He, Y. Hu, and Y. Liu, "Dispensing robot for toxic drugs in pharmacy intravenous admixture services," in *Proc. IEEE Int. Conf. Real-time Comput. Robot. (RCAR)*, Jul. 2021, pp. 905–909.

[19] *Esco | Class II, Type A2 Biological Safety Cabinets (E-Series)*. Accessed: Apr. 2, 2024. [Online]. Available: https://escolifesciences.co.kr/product/LA2-E/

[20] Y.-B. Bang, Y. S. Cho, S. H. Kong, J. Yoon, Y. L. Kim, R. H. Jung, and S. R. Lee, "A device for automation of drug liquid movement using a syringe," KR Patent 102 568 936 B1, Aug. 16, 2023.

[21] R. Hartenberg and J. Danavit, *Kinematic Synthesis of Linkages*. New York, NY, USA: McGraw-Hill, 1964.

[22] S. Kumar. (2018). *Kinematic Analysis of a WATT—II Slider Mechanism*. Accessed: Apr. 4, 2024. [Online]. Available: http://idr.nitkkr.ac.in:8080/xmlui/handle/123456789/2243

[23] K. S. Sollmann, "Modeling, simulation and control of a belt driven, parallel H-frame type two axes positioning system," M.S. thesis, Univ. Rhode Island, Kingston, RI, USA, 2007. [Online]. Available: https://doi.org/10.23860/thesis-sollmann-klaus-2007

[24] K. S. Sollmann, M. K. Jouaneh, and D. Lavender, "Dynamic modeling of a two-axis, parallel, H-frame-type XY positioning system," *IEEE/ASME Trans. Mechatronics*, vol. 15, no. 2, pp. 280–290, Apr. 2010.

[25] Y. Hwang, Y. Minami, and M. Ishikawa, "Virtual torque sensor for low-cost RC servo motors based on dynamic system identification utilizing parametric constraints," *Sensors*, vol. 18, no. 11, p. 3856, Nov. 2018.

[26] Y. Zhang, Z. Dou, J.-C. Veilleux, G. H. Shi, D. S. Collins, P. P. Vlachos, S. Dabiri, and A. M. Ardekani, "Modeling cavitation bubble dynamics in an autoinjector and its implications on drug molecules," *Int. J. Pharmaceutics*, vol. 608, Oct. 2021, Art. no. 121062.

[27] J.-C. Veilleux and J. E. Shepherd, "Pressure and stress transients in autoinjector devices," *Drug Del. Transl. Res.*, vol. 8, no. 5, pp. 1238–1253, Oct. 2018.

[28] J. Eshraghi, J.-C. Veilleux, G. Shi, D. Collins, A. M. Ardekani, and P. P. Vlachos, "Assessment of cavitation intensity in accelerating syringes of spring-driven autoinjectors," *Pharmaceutical Res.*, vol. 39, no. 9, pp. 2247–2261, Sep. 2022.

[29] J.-C. Veilleux, K. Maeda, T. Colonius, and J. E. Shepherd, "Transient cavitation in pre-filled syringes during autoinjector actuation," in *Proc. Int. Symp. Cavitation*, 2018, pp. 1–6.

[30] (Mar. 2023). *Moody Chart*. Accessed: Apr. 4, 2024. [Online]. Available: https://en.wikipedia.org/wiki/Moody_chart

[31] J. Kestin, M. Sokolov, and W. A. Wakeham, "Viscosity of liquid water in the range −8 °C to 150 °C," *J. Phys. Chem. Reference Data*, vol. 7, no. 3, pp. 941–948, Jul. 1978.

[32] R. L. Carey and D. H. Cromer, "The effect of buoyancy on weight and mass determinations," *Sci. Activities, Classroom Projects Curriculum Ideas*, vol. 5, no. 1, pp. 44–46, Feb. 1971.

[33] J. K. Taylor and H. V. Oppermann, *Handbook for the Quality Assurance of Metrological Measurements*, vol. 13. Gaithersburg, MD, USA: National Bureau of Standards, 1986.

[34] R. M. Schoonover and F. E. Jones, "Air buoyancy correction in high-accuracy weighing on analytical balances," *Anal. Chem.*, vol. 53, no. 6, pp. 900–902, May 1981.

[35] C. Bardin, A. Astier, A. Vulto, G. Sewell, J. Vigneron, R. Trittler, M. Daouphars, M. Paul, M. Trojniak, and F. Pinguet, "Guidelines for the practical stability studies of anticancer drugs: A European consensus conference," *Annales Pharmaceutiques Françaises*, vol. 69, no. 4, pp. 221–231, Jul. 2011.

[36] T. H. Geersing, M. G. Klous, E. J. F. Franssen, J. J. G. van den Heuvel, and M. Crul, "Robotic compounding versus manual compounding of chemotherapy: Comparing dosing accuracy and precision," *Eur. J. Pharmaceutical Sci.*, vol. 155, Dec. 2020, Art. no. 105536.

[37] T. Iwamoto, T. Morikawa, M. Hioki, H. Sudo, D. Paolucci, and M. Okuda, "Performance evaluation of the compounding robot, APOTECAchemo, for injectable anticancer drugs in a Japanese hospital," *J. Pharmaceutical Health Care Sci.*, vol. 3, no. 1, pp. 1–8, Dec. 2017.

JOANNE YOON (Member, IEEE) received the B.S. degree in mechanical system design engineering from Seoul National University of Science and Technology, Seoul, Republic of Korea, in 2016, and the Ph.D. degree in biomedical radiation sciences from Seoul National University, Seoul, in 2024. Currently, she works as a Research Assistant Professor with the Biomedical Research Institute, Seoul National University Hospital, where her research focuses on the design and control of medical robots.

YE-LIN KIM received the B.S. degree in information and control, division of robotics from Kwangwoon University, Seoul, in 2022. She is currently pursuing the Ph.D. degree with the Department of Applied Bioengineering, Graduate School of Convergence Science and Technology, Seoul National University. Her research interests include theoretical and applied research in the medical robotics field with commander–responder architectures.

YOUNG-BONG BANG (Senior Member, IEEE) received the B.S. and M.S. degrees in mechanical engineering from Seoul National University, Seoul, Republic of Korea, in 1989 and 1991, respectively, and the Ph.D. degree in precision machinery engineering from the University of Tokyo, Tokyo, Japan, in 1997. He worked for FANUC Ltd., from 1997 to 1999, the School of Mechanical and Aerospace Engineering, Seoul National University from 2000 to 2009, and the Advanced Institute of Convergence Technology from 2009 to 2020. Since August 2020, he has been with Seoul National University Hospital. His research interests include actuator-based mechatronic systems, medical robotics, and assistive technology.